Two-dimensional spectroscopy of a molecular dimer unveils the effects of vibronic coupling on exciton coherences

December 7, 2014

Alexei Halpin[1], Philip J. M. Johnson[1], Roel Tempelaar[2], R. Scott Murphy[3], Jasper Knoester[2], Thomas L. C. Jansen[2], & R. J. Dwayne Miller[1,4].

[1] Institute for Optical Sciences and Departments of Chemistry and Physics, University of Toronto, 80 St. George Street, Toronto, Ontario M5S 3H6, Canada.
[2] Zernike Institute for Advanced Materials, University of Groningen, Nijenborgh 4, 9747 AG Groningen, The Netherlands.
[3]Department of Chemistry and Biochemistry, University of Regina, 3737 Wascana Parkway, Regina, SK, S4S 0A2, Canada.
[4]Max Planck Institute for the Structure and Dynamics of Matter, Atomically Resolved Dynamics Division Building 99 (CFEL), Luruper Chaussee 149, 22761 Hamburg, Germany.

Abstract

The observation of persistent oscillatory signals in multidimensional spectra of protein-pigment complexes has spurred a debate on the role of coherence-assisted electronic energy transfer as a key operating principle in photosynthesis. Vibronic coupling has recently been proposed as an explanation for the long lifetime of the observed spectral beatings. However, photosynthetic systems are inherently complicated, and tractable studies on simple molecular compounds are in demand to fully understand the underlying physics. In this work, we present measurements and calculations on a solvated molecular homodimer with clearly resolvable oscillations in the corresponding two-dimensional spectra. Through analysis of the various contributions to the nonlinear response, we succeed in isolating the signal due to inter-exciton coherence. We find that while calculations predict a prolongation of this coherence due to vibronic coupling, the combination of dynamic disorder and vibrational relaxation leads to a coherence decay on a timescale comparable to the electronic dephasing time.

1 Introduction

Recent advances in ultrafast nonlinear spectroscopy have revived the discussion on the role of quantum dynamics in biological photosynthesis [1–3]. The extension of two-dimensional (2D) spectroscopy to the visible range [4] has allowed light-harvesting complexes to be investigated in great detail [5, 6], revealing electronic energy transfer between the coupled pigments [5, 7]. The observation of long-lasting oscillatory features in 2D spectra of the Fenna-Matthews-Olson (FMO) complex [8] has stimulated the hypothesis that this transfer happens coherently. In this picture a coherent superposition of excited states, responsible for the observed oscillations, samples the most efficient route towards the reaction centre in a more rapid way than would be possible by diffusive, incoherent excitation energy transfer. This idea found further support in a subsequent series of measurements that showed spectral beatings for cryptophyte algae [3] and Photosystem II protein complexes [9], indicating that coherent behavior in biological systems is ubiquitous. For FMO, the oscillations were found to persist for hundreds of femtoseconds at ambient temperatures and even up to a few picoseconds at 77 K [10]. In contrast, the measured spectral linewidths predict electronic dephasing times at 77 K hardly exceeding 100 fs [11], owing to rapid, stochastic variations

in the environment, and coherences between excitons are expected to decay roughly on this timescale. The long coherence times could be explained by correlations between the fluctuating electronic site transition energies, but these are not concordant with recent molecular dynamics simulations [12, 13].

Over the last year, several independent publications alluded to vibronic coupling as an explanation for long-lived spectral beatings [14–16]. Coupling of electronic transitions to an underdamped vibrational mode may result in inter-exciton coherences with strong intra-pigment character, that is, consisting of wavepackets in different vibrational levels on the same chromophore. Due to the inherent correlation of these levels, such coherences will experience an extended dephasing time. For FMO, the Huang-Rhys factors are very small, suggesting that the corresponding photophysics is primarily electronic in nature, yet calculations using a vibronic exciton model nevertheless predicted an inter-exciton dephasing on the order of picoseconds [14]. As such, vibronic coupling acts as a mechanism to conserve electronic coherence. Earlier even, vibronic coupling combined with dynamic disorder was theoretically shown to possibly lead to enhanced transport in cyanobacterial light-harvesting proteins [17].

Vibronic coupling is an omnipresent phenomenon [18], both in synthetic and biological systems, yet in the context of ultrafast spectroscopy it forms a relatively unexplored area. For FMO, several Franck-Condon active vibrations are found with frequencies in the range of 0 to 350 cm^{-1} [11, 19]. Similar low-frequency phonons contribute to the observed dynamics of retinal proteins involved in vision [20, 21]. There, the importance of vibronic coupling follows intuitively from the structural change experienced by the chromophores, implicating a number of highly delocalized skeletal modes needed for isomerization. In photosynthetic aggregates, on the other hand, no such explicit connection to the biologically relevant energy transfer process is present. The above-mentioned accounts on FMO suggest an effect of vibronic coupling on exciton coherences, but these theoretical efforts remain to be reinforced

with specific experimental verification. The main difficulty is that biological molecules are typically too complicated to allow for an unambiguous interpretation of spectral beatings. In the purely electronic representation alone, the 2D spectrum of a pigment complex contains a multitude of congested diagonal and off-diagonal peaks. Only very recently, coherent oscillations have been investigated in the context of small synthetic aggregates [22]. However, even for such simple molecules, vibronic coupling automatically gives rise to additional oscillating coherences of ground state vibrational wavepackets that might overlap with excited state features [16, 23, 24]. Studies aimed at disentangling vibrational and excitonic coherences in such cases have focused on limiting examples of purely vibrational and electronic excitations, and have not led to a consensus method for their distinction in measurements, without loss of generality [25, 26].

In this paper, we present a joint experimental and theoretical study on the effect of strong vibronic coupling on coherences between excitons. Measurements are performed on a theoretically tractable homodimer with well-separated spectral features. Certain distinctions must be made between this model system and photosynthetic pigment complexes. In the latter case, the pigments are also identical, albeit more weakly coupled, and frequently possess static disorder in the site energies set by the environment, which renders such complexes inherently asymmetric. The homodimer presented here does possess symmetry with respect to interchange of both chromophores, however local dynamic fluctuations in the environment will act to break this symmetry producing an inhomogeneous distribution of site energies. The measured spectral peaks are found to exhibit clear periodic beatings. Most of these peaks consist of overlapping features, however, via the accompanying calculations in the vibronic exciton model, we are able to assign the spectral contribution stemming from a coherence of the two most radiant excited states. The theoretical model elucidates how inter-exciton coherence is enhanced in time through a mixing with vibrational degrees of freedom, and our comparison to measured data allows us to investigate such enhancement

in a realistic molecular system.

2 Results and Discussion

2.1 Vibronic excitons of a cyanine dimer

The results presented in this paper are obtained for a dimer of identical indocarbocyanine molecules covalently bound via two butyl chains [27], studied at room temperature. The corresponding molecular structure is depicted in Fig. 1a. The linear absorption spectrum of the monomer subunits (see Supplementary Fig. 1) features a pronounced vibronic progression due to strong coupling of the S_0-S_1 electronic transition to a C-C stretching mode in the polymethine chain [28]. In the dimer compound, electronic interactions cause a delocalization of the vibronic excitations over the two monomers, leading to polaronic Frenkel excitons

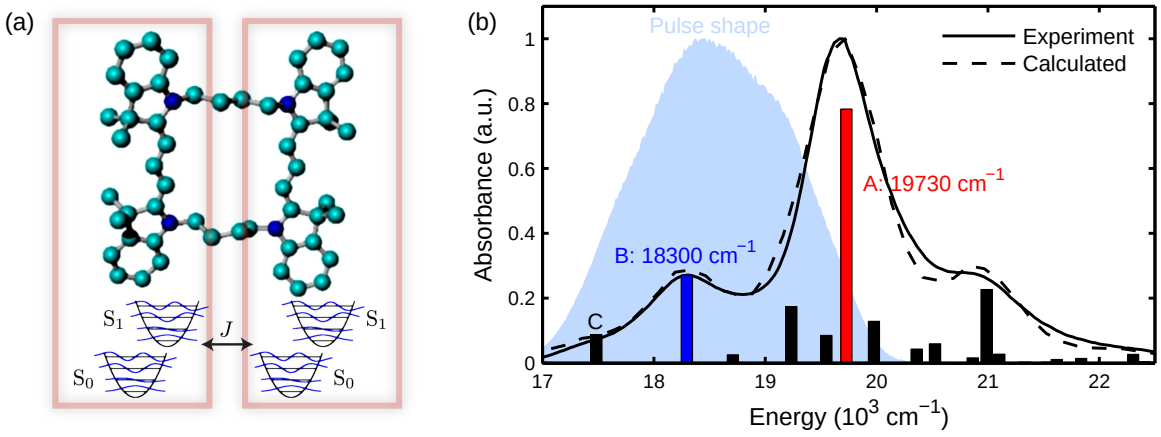

Figure 1: Modeling the linear absorption spectrum of indocarbocyanine. (a) Chemical structure of the biscyanine compound (teal/blue balls represent carbon/nitrogen atoms, hydrogen atoms not shown). A cartoon depiction of the two types of interactions primarily contributing to the photophysics of the dimer is shown below: the chromophores interact via excitonic coupling J, while each subunit experiences vibronic coupling as depicted by the displacements between the S_0 and S_1 vibrational potentials. (b) Measured (solid curve) and calculated (dashed) absorption spectrum of the compound, together with the calculated stick spectrum depicting the transitions contributing to the lineshape. Also shown is the laser spectrum (filled blue area), used to acquire the 2D spectra.

[18, 29, 30]. These excited states depend critically on the molecular geometry, notably the distance and relative angular orientation between the subunits, which are calculated to be 10 Å and 15 degrees in vacuum (using the PM3 and MM+ optimizations in HyperChem v. 7 [31]). Shown in Fig. 1b is the experimental linear absorption spectrum of the dimer (solid curve), which in turn is determined by the total contribution of collective excited states. The linear absorption measurements of both the monomer and dimer are well reproduced using the vibronic exciton model as formulated by the Holstein Hamiltonian [29], which is evaluated using the two-particle approximation [32,33] (details given in Supplementary Section 2). The best agreement between calculations and experiments is found using an excitonic coupling strength of 800 cm^{-1}, while the vibronic coupling is described using a vibrational frequency of 1220 cm^{-1} and a Huang-Rhys factor of 0.58. The solvent is incorporated by coupling the electronic transition energies of the individual chromophore subunits to a coordinate, which performs Gaussian-stochastic fluctuations corresponding to an exponential correlation function [34] with a standard deviation of 500 cm^{-1} and a decay time of 40 fs. The calculated linear absorption of the dimer is shown as dashes in Fig. 1b (a fit to the monomer variant is included in the Supplementary Fig. 1).

From the calculated stick spectrum, shown in Fig. 1b, it is evident that there is a great number of transitions underneath the broad linewidth of the absorption spectrum. Nevertheless, two excited states are easily recognized as carrying the bulk of the oscillator strength. The most absorbant of the two is located around 19730 cm^{-1} (red stick), the second at 18300 cm^{-1} (blue stick). These states, which will be referred to as A and B, respectively, are expected to dominate the 2D spectra even more, since in that case peak intensities are determined by roughly the oscillator strength squared. We note that a third strongly radiant state resides in the blue tail of the spectrum. As will be shown later on, this state has a negligible contribution to the spectral dynamics studied in this work. The high intensity of states A and B can be understood from Fig. 2, which shows a selection of the corresponding

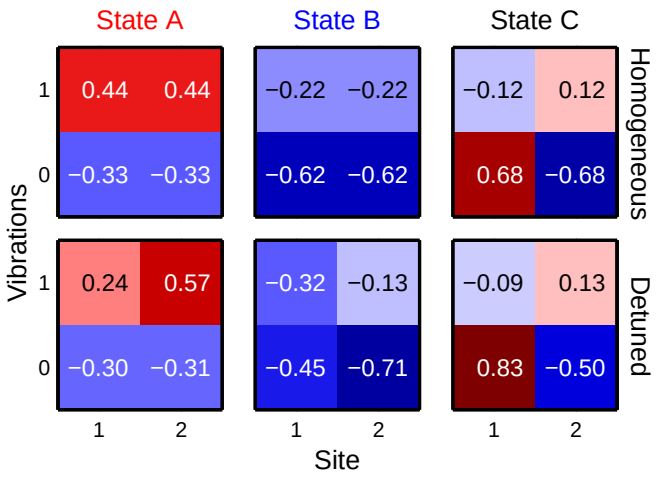

Figure 2: The effect of energy fluctuations on states A, B and C. Tables summarize the calculated wavefunction coefficients as a function of the chromophore site (horizontally) and the number of vibrational quanta (vertically). For each cell, the background color emphasizes the sign of the coefficient being positive (red) or negative (blue). When the S_0-S_1 transition energies of the sites are equal (homogeneous, top row), states A and B are both composed of symmetric wavefunctions inside the vibronic bands. When the energy of site 1 is lowered by 500 cm^{-1} (detuned, bottom row), both states tend to localize on the same pigment. As such, states A and B perform correlated fluctuations when subject to disorder. Only coefficients are shown of single-particle basis states including 0 and 1 phonons (see Supplementary Section 2 for details).

wavefunction coefficients in the local basis. Instead of disorder-averaged values, cases are shown where the electronic transition energies of the sites are homogeneous (top row), and where these energies are detuned with respect to each other (bottom row). For the moment restricting our attention to the homogeneous case, we observe that each vibrational band is occupied by a wavefunction that is symmetrically delocalized over both sites. This leads to constructive interference for the oscillator strength, similar to what is observed for a purely electronic dimer (usually referred to as superradiance [35]). Fig. 2 also shows the characterization of state C, located in the low-energy tail of the absorption spectrum, which in contrast is only weakly absorbing since it consists of "dark" antisymmetric wavefunctions.

To a good approximation, states B and C reduce to a symmetric and antisymmetric pair in the 0-phonon band. When the site energies of the dimer are subject to a detuning,

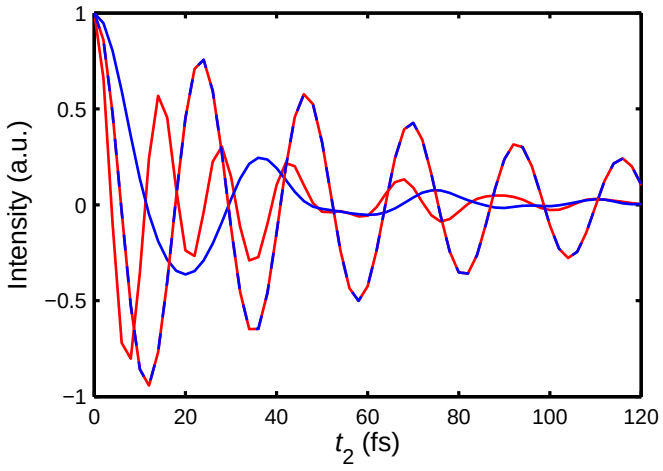

Figure 3: Temporal enhancement of inter-exciton coherence. Shown are calculated coherences between states A and B (red-blue), states A and C (red), and states B and C (blue) as a function of time t_2. As states A and B fluctuate in a correlated fashion, their mutual coherence experiences an extended dephasing time.

these states tend to localize on opposite pigments, that is, B and C become trapped at the higher- and lower-energy site, respectively. Much like B, state A also reduces to a symmetric wavefunction, but mainly localized in the 1-phonon band. Interestingly, detuning causes this wavefunction to become trapped on the same site as was found for state B. In the dynamic picture, the pigment transition energies fluctuate with respect to each other, and in this process the homogeneous case (top row), where states A and B are both delocalized, and the detuned case (bottom row), where states A and B are localized on the same pigment, will interchange. As such, both states will fluctuate in a correlated fashion, and hence their mutual coherence is expected to be robust against homogeneous dephasing. This is verified by Fig. 3, which shows the calculated A-B coherence for the dimer in the dynamic solvent environment (red-blue curve). A corresponding $1/e$ decay time of 80 fs is found; well beyond the homogeneous dephasing time, which is experimentally predicted to be roughly 40 fs (as demonstrated in Supplementary Section 1). In marked contrast, due to trapping at opposite sites, the A-C and B-C pairs do not experience such a correlation, and the calculated coherences decay within the homogeneous dephasing time (red and blue curve,

respectively). It should be noted that the coherences reported here can not be referred to as purely electronic or vibrational, but rather as vibronic, since the electronic and vibrational degrees of freedom have become nontrivially mixed.

2.2 Two-dimensional spectroscopy

The temporal enhancement of the A-B coherence due to vibronic coupling is consistent with the theoretical predictions made in Refs. [14] and [15], despite the differences in excitonic and vibronic coupling. Moreover, the cyanine dimer considered here forms the perfect model system to experimentally address these predictions, given that the strong couplings lead to well-resolved crosspeaks, and that states A and B dominate the nonlinear response. Both of these aspects are immediately borne out in the experimental 2D correlation spectrum (at waiting time $t_2 = 0$) shown in Fig. 4a. Here, ω_1 and ω_3 denote the excitation and detection energies, respectively. Two positive peaks are present along the diagonal, which appear at the same frequencies as in the linear absorption. These correspond to the ground state bleach (GB) and stimulated emission (SE) contributions due to states A and B. Between both diagonal features we observe two crosspeaks. The one above the diagonal is almost completely masked by two negative peaks stemming from excited state absorption (EA), of which the most prominent is denoted by X in Fig. 4a. In the 2D spectra measured at different waiting times, we find multiple oscillating features with dramatic beatings continuing for about 70 fs following excitation (see Supplementary Fig. 2 for a series of experimental 2D spectra). This is especially so at X, where the signal changes sign with a period of roughly 23 fs.

The 2D spectra have been acquired using the laser pulse depicted in Fig. 1b. This laser spectrum somewhat mitigates the prevalence of signals associated with the large transition dipole of state A by only weakly overlapping with that peak, while enhancing the relative contribution of peak B. Through calculations on electronic dimers, Kjellberg and coworkers

have demonstrated that at waiting times exceeding the pulse duration, realistic pulse envelopes mostly act as a frequency filter in 2D spectra [36]. Even in the presence of vibronic coupling, the expected effect of the pulse spectrum is mainly the suppression or enhancement of spectral peaks. This is supported by accompanying calculations in the impulsive limit, which clearly demonstrate the essential features apparent in the experiments (a comparison to the measurements is included in Supplementary Fig. 2). Notably, the intense dynamics at peak X are conspicuous in both in the measured and calculated spectra.

In Ref. [37], it has been shown for weak excitonic and vibronic coupling that the conservation of coherence due to mixing with vibrational degrees of freedom works optimally when the vibrational quantum is resonant with the splitting between electronic energies. Such is the case for FMO, where an underdamped bath mode with an energy of 185 cm^{-1} matches the splitting between the lowest-energy pigment and one of its neighbors [14]. However, all molecular systems that fulfill this resonance criterion share the problem that most excited state coherences considerably overlap with contributions to the 2D spectra arising from vibrational wavepackets. In the biscyanine dimer a similar overlap occurs, since the 1220 cm^{-1} mode roughly bridges the energies between states A and B (which will be referred to as ω_{A} and ω_{B}), leading to intense oscillations due to ground state phonons at the excitonic crosspeak positions. These observations reinforce that one should be extremely careful in the assignment of spectral beats, even with well-separated spectral features as in the present dimer system. This point is of even greater importance in the case of more complicated (biological) molecules, where the broad diagonal peaks typically undergo periodic lineshape modulations due to low-frequency vibrations [38,39] that can easily be mistaken for coherent oscillations due to excitons.

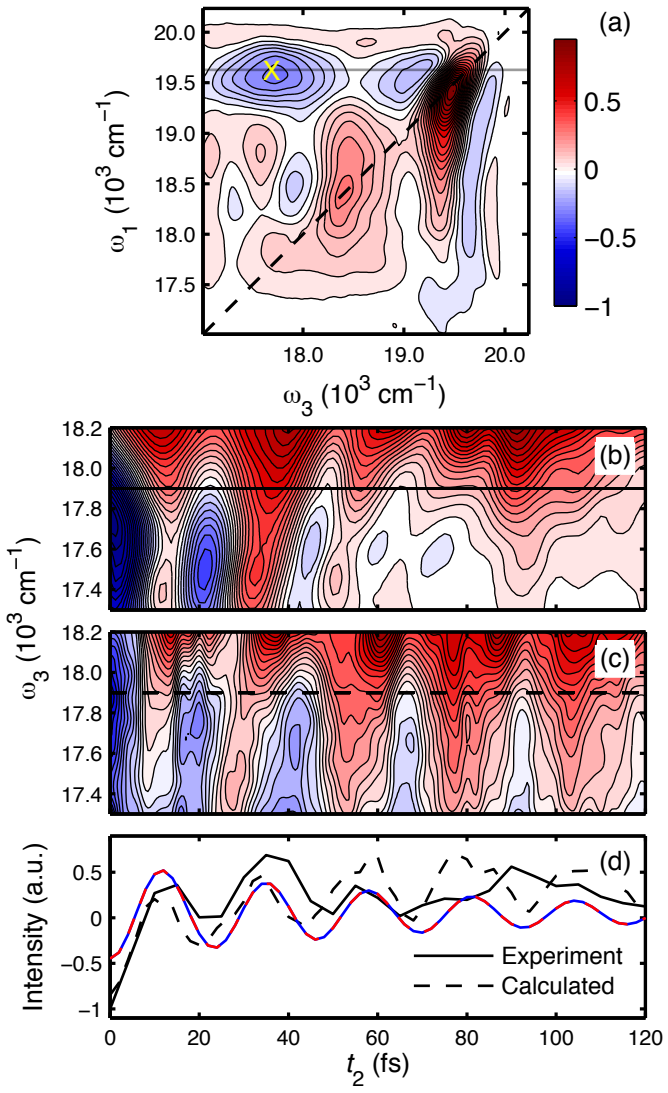

Figure 4: Signatures of inter-exciton coherence in 2D spectroscopy. (a) Measured real-valued correlation spectrum (at $t_2 = 0$) with grey horizontal line indicating the region from which the dynamics (shown in the panel below) are extracted (contour lines at 5% intervals). (b) Spectrally resolved slice of the experimentally obtained correlations between pumping at A and recording the nonrephasing signal at other frequencies. The frequency corresponding to peak X is indicated by the horizontal line. (c) Calculated analogue of (b). (d) Both the experimental (solid curve) and numerical (dashed) trace of X exhibit the same periodicity as the calculated A-B coherence (red-blue curve).

2.3 Spectral signatures of inter-exciton coherence

For the spectral window studied here, our calculations have indicated contributions from purely vibrational coherences to be dominant in the rephasing signal, in marked contrast to the nonrephasing (NR) spectra, where ground state phonons only contribute significantly in the diagonal region. Particularly the NR signal at peak X is to a great extent determined by excited states. This peak results from pumping at state A, as it is located at $\omega_1 = \omega_{\mathrm{A}}$. Shown in Fig. 4b is the t_2-dependent "slice" of the measured nonrephasing signal, spectrally resolved in ω_3 and corresponding to excitation at ω_{A}. Different oscillating contributions are clearly apparent in this spectral slice, which are well accounted for by the numerical reproduction shown in Fig. 4c. The probe frequency of X corresponds to $\omega_3 = 17900$ cm^{-1}, and is indicated by the solid and dashed lines in the experimental and calculated slices, respectively. The time series of these line profiles are shown in Fig. 4d, and essentially indicate the amplitude of X as a function of t_2. For this amplitude, the agreement between the measurements and calculations is strong for a waiting time up to about 70 fs, and in both cases we observe a pronounced oscillation with a frequency of approximately 1400 cm^{-1}. From the close resemblance of the 17900 cm^{-1} probe frequency to the energy of state C (recall Fig. 1), one might expect this beating to arise from the A-C coherence. However, the oscillator strength of C is simply too small for this state to significantly contribute to the 2D spectrum. Instead, peak X very accurately indicates the A-B coherence, as is already hinted at by the agreement between the observed oscillation frequency and the A-B splitting. For comparison, the calculated A-B coherence is also shown in Fig. 4d (red-blue curve), and is in good agreement with the measured and calculated traces.

The fact that peak X serves as an indicator of the A-B coherence is demonstrated numerically in Fig. 5. Panel (a) shows the total NR trace at X (black curve), together with the NR contributions from GB (green), SE (red) and EA (blue), for a homogeneous dimer. The SE and EA signals clearly oscillate with the same frequency, in contrast to the GB contribution

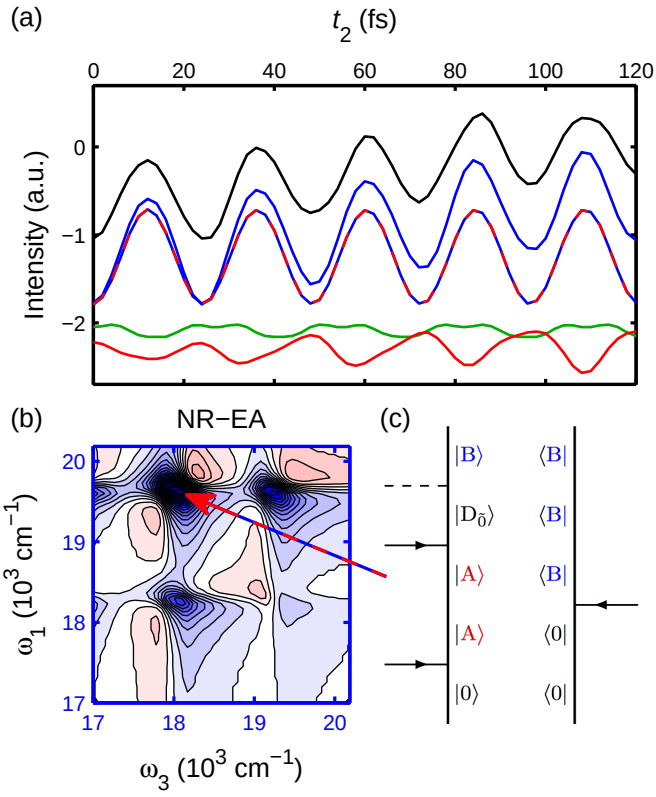

Figure 5: Decomposition of the different pathways contributing to peak X. (a) Calculated nonrephasing trace of peak X for a homogeneous dimer (black), together with the contributions from GB (green), SE (red) and EA (blue). Also shown is the corresponding A-B coherence (red-blue). (b) Calculated NR-EA correlation spectrum. Arrow points the feature that predominantly contributes to X, and which indicates the A-B coherence via the pathway of the system's density operator illustrated in (c). In this pathway, $D_{\tilde{0}}$ denotes the doubly excited state involving a total of zero phonons.

that exhibits a beating pattern with a different periodicity. This beating is generally too weak to significantly contribute to the total NR trace, which is predominantly determined by the EA signal. Unlike the other reported calculations, the results presented in this figure have been calculated through a sum-over-states approach (see Supplementary Section 2 for details), which allows to include only specific states. This has been employed to demonstrate that the NR-EA signal is determined almost solely by states A and B (red-blue curve). In other words, peak X serves as an accurate measure of the A-B coherence. Further analysis has shown that this coherence is mainly contributing through the NR-EA pathway illus-

trated in Fig. 5c, giving rise to the feature highlighted in Fig. 5b. Note that, while the peak energy of the A $\rightarrow$ $D_{\tilde{0}}$ transition is calculated to be on the red of our experimental spectral window, the width of that transition and its large transition dipole moment nevertheless lead to its presence under these excitation conditions (effects pertaining to the spectral weighting occurring in the experiment are further discussed in Supplementary Section 1). The analysis in Fig. 5 additionally demonstrates that the higher-energy state, while strongly present in the blue tail of the linear absorption spectrum, does not yield a significant contribution in the vicinity of X, even in the impulsive limit.

The enhancements in coherence times due to vibronic coupling have been discussed so far in relation to completely undamped modes [14, 15, 37]. Also in our theoretical model, the vibrational levels are assumed to be entirely correlated. The reason for the calculated A-B coherence having a dephasing time of 80 fs, instead of the super-picosecond timescale predicted for FMO in Ref. [14], is the strong disorder present in the model. While FMO at 77 K has a characteristic disorder width of about 60 cm^{-1} [5], the biscyanine compound is surrounded by room temperature fluctuations as strong as 500 cm^{-1}. Even so, the calculations overestimate the experimental A-B coherence time as measured at peak X. A plausible explanation for this discrepancy is a fast relaxation pathway occurring for the 1220 cm^{-1} vibrational mode. This idea is supported by the fact that, in the measured 2D spectra, no oscillations are found after $t_2 = 100$ fs. Were the vibration conserved, ground state vibrational wavepackets would continue to contribute beating signals for extremely long times. An additional indication of vibrational relaxation is provided by pump-probe measurements, which do not show the robust oscillations one would expect from an undamped phonon (as illustrated by data presented in Supplementary Figs. 3 and 4).

3 Conclusion

The signatures of vibronic coupling in multidimensional spectroscopy have drawn great interest lately, in particular to interpret oscillatory transients observed for light-harvesting complexes [3, 8–10] that persist much longer than predicted electronic dephasing times [11]. For such molecular systems, where vibronic coupling acts in concert with electronic interactions, the vibronic exciton model forms an indispensable tool to understand the underlying dynamical processes. In this work, we demonstrate the first direct application of this model to experimental 2D spectra on a homodimer system. The importance of such a comparative study of measured results and the expected response based on calculations becomes immediately evident: even in a strongly coupled system where 2D spectral features are well-resolved, a multitude of dynamic contributions overlap in a nontrivial way. In particular, oscillatory signals associated with ground state vibrational wavepackets are strongly present at excitonic crosspeak locations, as was already emphasized by earlier studies [16, 23–26]. Using numerical predictions, we nevertheless managed to accurately extract the coherence between the two most radiant states of the homodimer system through excited state absorption features.

This study impacts on the recent theoretical studies on FMO [14–16, 37], which have suggested that vibronic coupling to an undamped mode acts to correlate excited states, as an explanation of long-lived coherences observed as off-diagonal beats in experiments. Our calculations show for the two strongest absorbing excitons that the dephasing effect of site disorder is negated by a localization on the same pigment. It should be noted that the resulting long-lived coherence largely reflects the dynamics within this single pigment, and hence the relation of the corresponding spectral beatings to energy transfer is far from trivial. Moreover, the experimental results show a coherence decay on the order of the homogeneous dephasing time, which likely has contributions from the relaxation of the associated vibrational mode. Hence, this work highlights that while vibronic enhancement of dephasing

times can occur, its operation depends on the system-bath coupling and robustness of the vibration, which is strongly dependent on the molecular system in question.

4 Methods

The biscyanine was prepared following reported procedures [40–42]. Initially, the compound was recrystallized from methanol/0.5M $NaBF_4$. A final recrystallization from dichloromethane/heptane with small amounts of tetrahydrofuran and toluene gave purple crystals. HRMS-ESI (m/z): $[M]^+$ calculated for $C_{54}H_{62}BF_4N_4$, 852.5034; found, 852.5035. Anal. Calculated for $C_{54}H_{62}N_4B_2F_8{\cdot}NaBF_4$: C, 61.74; H, 5.95; N, 5.33. Found: C, 61.68; H, 5.42; N, 5.13. All values are given as percentages.

The sample was dissolved in methanol and circulated through a homebuilt flow cell via a gear pump. The sample OD at 547 nm is ~ 0.25 for a 400 μm path length. Measurements were performed using the 2D spectrometer described in detail previously [43]. The femtosecond laser system consists of an Er-doped fibre oscillator (Delmar Photonics, USA) which seeds a homebuilt Ti:Sapphire regenerative amplifier, the output of which is used to pump a noncollinear optical parametric amplifier.

Phase distortions across the excitation spectrum were corrected using a combination of fused silica prisms and a deformable mirror (OKOTech, Netherlands) based pulse shaper. Pulse compression was monitored in a dedicated transient-grating based frequency-resolved optical gating setup [44], and the pulse profile was also measured in the 2D setup. For the 2D spectra presented here the pulse duration was 16 fs as measured *in situ*. In the 2D spectrometer, a diffractive optic element (INO, Canada) was used to generate phase locked pairs of beams and the temporal delays t_1 and t_2 were controlled via retroreflectors mounted on motorized delay stages (Newport, USA). Before entering the setup, the p-polarized input pulses were sent through a wave plate (Special Optics, USA) and polarizer (Moxtek, USA)

to control the incident power. This allows to excite the sample in the linear regime. To verify this, the magnitude of homodyne response from the sample was recorded for different incident fluences, and measured using a power meter (Fieldmaster, Coherent, USA). In the measurements above the incident energy was $\sim$ 5 nJ (per excitation beam), with a focal spot size of approximately 50 μm, corresponding to a maximum peak intensity [45] of 30 GW/cm^2 when all pulses are temporally overlapped in the sample. The heterodyne detected photon-echo signals were collected along a temporal window of $t_1 = \pm$ 128 fs in steps of 1 fs. The LO pulse was attenuated by two orders of magnitude and delayed by approximately 420 fs relative to the pulses used to generate the echo.

Calculations in the vibronic exciton model were performed by combining the Holstein Hamiltonian [29] with the Numerical Integration of the Schrödinger Equation method [46,47]. The latter relies on the response function approach [34], and simulates 2D spectra in the impulsive limit. The two-particle approximation was employed for the quantum basis set, which for a dimer system is equivalent to the full basis (convergence is assured with respect to truncation of the total number of vibrational quanta). The solvent environment was modelled through Gaussian-stochastic fluctuating classical coordinates that linearly couple to the chromophore electronic transition energies. No back-reaction of the chromophores onto the coordinates was accounted for, leading to a neglect of the dynamic Stokes shift and a relaxation towards equally populated quantum states (high-temperature limit). A study on a comparable molecular dimer [48] has suggested that such leads to minor discrepancies in the timeframe studied in the current work. Reported numerical linear and nonlinear spectra were sampled over 10,000 disorder trajectories. The calculated inter-exciton coherences were sampled over 500,000 trajectories. Further analysis was performed using a sum-over-states approach (details in Supplementary Section 2).

5 Acknowledgments

We are grateful to Valentyn Prokhorenko, Harald Kauffmann and Frank Spano for helpful discussions regarding interpretation of the results, and Etienne Pelletier for assistance with the laser system. Financial support provided by the Natural Sciences and Engineering Research Council of Canada (NSERC) (R.S.M., R.J.D.M.) and the Max Planck Society (R.J.D.M.).

6 Author contributions

A.H. and P.J.M.J. performed the measurements. R.T. and T.L.C.J. performed the calculations. A.H., R.T., P.J.M.J., T.L.C.J. analyzed the data. A.H. constructed the experimental setup. R.S.M. synthesized the compound. A.H. and R.T. wrote the manuscript, and R.J.D.M. and J.K. supervised the project.

7 Corresponding author

Correspondence and requests for materials should be directed to R.J.D.M.

(dwayne.miller@mpsd.cfel.de)

References

[1] Sundström, V. Femtobiology. *Annu. Rev. Phys. Chem.* **59**, 53–77 (2008).

[2] Cheng, Y. C. & Fleming, G. R. Dynamics of light harvesting in photosynthesis. *Annu. Rev. Phys. Chem.* **60**, 241–262 (2009).

[3] Collini, E. *et al.* Coherently wired light-harvesting in photosynthetic marine algae at ambient temperature. *Nature* **463**, 644–647 (2010).

[4] Hybl, J. D., Albrecht, A. W., Gallagher Faeder, S. M. & Jonas, D. M. Two-dimensional electronic spectroscopy. *Chem. Phys. Lett.* **297**, 307–313 (1998).

[5] Brixner, T. *et al.* Two-dimensional spectroscopy of electronic couplings in photosynthesis. *Nature* **434**, 625–628 (2005).

[6] Schlau-Cohen, G. S. *et al.* Elucidation of the timescales and origins of quantum electronic coherence in LHCII. *Nature Chem.* **4**, 389–395 (2012).

[7] Myers, J. A. *et al.* Two-dimensional electronic spectroscopy of the D1-D2-cyt b559 photosystem II reaction center complex. *J. Phys. Chem. Lett.* **1**, 2774–2780 (2010).

[8] Engel, G. S. *et al.* Evidence for wavelike energy transfer through quantum coherence in photosynthetic systems. *Nature* **446**, 782–786 (2007).

[9] Ishizaki, A., Calhoun, T. R., Schlau-Cohen, G. S. & Fleming, G. R. Quantum coherence and its interplay with protein environments in photosynthetic electronic energy transfer. *Phys. Chem. Chem. Phys.* **12**, 7319–7337 (2010).

[10] Panitchayangkoon, G. *et al.* Long-lived quantum coherence in photosynthetic complexes at physiological temperature. *Proc. Natl. Acad. Sci.* **107**, 12766–12770 (2010).

[11] Wendling, M. *et al.* Electron-vibrational coupling in the Fenna-Matthews-Olson complex of *Prosthecochloris aestuarii* determined by temperature-dependent absorption and fluorescence line-narrowing measurements. *J. Phys. Chem. B* **104**, 5825–5831 (2000).

[12] Abramavicius, D. & Mukamel, S. Exciton dynamics in chromophore aggregates with correlated environment fluctuations. *J. Chem. Phys.* **134**, 174504 (2011).

[13] Olbrich, C., Struempfer, J., Schulten, K. & Kleinekathoefer, U. Quest for spatially correlated fluctuations in the fmo light-harvesting complex. *J. Phys. Chem. B* **115**, 758–764 (2011).

[14] Christensson, N., Kauffmann, H. F., Pullerits, T. & Mančal, T. Origin of long-lived coherences in light-harvesting complexes. *J. Phys. Chem. B* **116**, 7449–7454 (2012).

[15] Chin, A. W. *et al.* The role of non-equilibrium vibrational structures in electronic coherence and recoherence in pigment-protein complexes. *Nature Phys.* **9**, 113–118 (2013).

[16] Tiwari, V., Peters, W. & Jonas, D. Electronic resonance with anticorrelated pigment vibrations drives photosynthetic energy transfer outside the adiabatic framework. *Proc. Natl. Acad. Sci.* **110**, 1203–1208 (2013).

[17] Womick, J. & Moran, A. Vibronic enhancement of exciton sizes and energy transport in photosynthetic complexes. *J. Phys. Chem. B* **115**, 1347–1356 (2011).

[18] Spano, F. C. The spectral signatures of Frenkel polarons in H- and J-aggregates. *Acc. Chem. Res.* **43**, 429–439 (2009).

[19] Rätsep, M. & Freiberg, A. Electron-phonon and vibronic couplings in the FMO bacteriochlorophyll a antenna complex studied by difference fluorescence line narrowing. *J. Lumin.* **127**, 251–259 (2007).

[20] Schoenlein, R. W., Peteanu, L. A., Mathies, R. A. & Shank, C. V. The 1st step in vision - femtosecond isomerization of rhodopsin. *Science* **254**, 412–415 (1991).

[21] Hou, B., Friedman, N., Ottolenghi, M., Sheves, M. & Ruhman, S. Comparing photoinduced vibrational coherences in bacteriorhodopsin and in native and locked retinal protonated Schiff bases. *Chem. Phys. Lett.* **381**, 549–555 (2003).

[22] Hayes, D., Griffin, G. B. & Engel, G. Engineering coherence among excited states in synthetic heterodimer systems. *Science* doi:10.1126/science.1233828 (2013).

[23] Christensson, N. *et al.* High frequency vibrational modulations in two-dimensional electronic spectra and their resemblance to electronic coherence signatures. *J. Phys. Chem. B* **115**, 5383–5391 (2011).

[24] Turner, D. B., Wilk, K. E., Curmi, P. M. G. & Scholes, G. D. Comparison of electronic and vibrational coherence measured by two-dimensional electronic spectroscopy. *J. Phys. Chem. Lett.* **2**, 1904–1911 (2011).

[25] Turner, D. B. *et al.* Quantitative investigations of quantum coherence for a light-harvesting protein at conditions simulating photosynthesis. *Phys. Chem. Chem. Phys.* **14**, 4857–4874 (2012).

[26] Butkus, V., Zigmantas, D., Valkūnas, L. & Abramavičius, D. Vibrational vs. electronic coherences in 2D spectrum of molecular systems. *Chem. Phys. Lett.* **545**, 40–43 (2012).

[27] Chibisov, A. K. *et al.* Photorelaxation processes in covalently linked indocarbocyanine and thiacarbocyanine dyes. *J. Phys. Chem.* **99**, 886–893 (1995).

[28] Mustroph, H. *et al.* Relationship between the molecular structure of cyanine dyes and the vibrational fine structure of their electronic absorption spectra. *ChemPhysChem* **10**, 835–840 (2009).

[29] Holstein, T. Studies of polaron motion: Part I. The molecular-crystal model. *Ann. Phys.* **8**, 325–342 (1959).

[30] Davydov, A. S. Solitons in molecular systems. *Phys. Scr.* **20**, 387–394 (1979).

[31] HyperChem v. 7. http://www.hyper.com/

[32] Philpott, M. R. Theory of the coupling of electronic and vibrational excitations in molecular crystals and helical polymers. *J. Chem. Phys.* **55**, 2039–2054 (1971).

[33] Spano, F. C. Absorption and emission in oligo-phenylene vinylene nanoaggregates: The role of disorder and structural defects. *J. Chem. Phys.* **116**, 5877–5891 (2002).

[34] Mukamel, S. *Principles of Nonlinear Spectroscopy* (Oxford University Press, Oxford, U.K., 1999).

[35] Fidder, H., Knoester, J. & Wiersma, D. Superradiant emission and optical dephasing in J-aggregates. *Chem. Phys. Lett.* **171**, 529–536 (1990).

[36] Kjellberg, P., Brüggemann, B. & Pullerits, T. Two-dimensional electronic spectroscopy of an excitonically coupled dimer. *Phys. Rev. B* **74**, 024303 (2006).

[37] Chenu, A., Christensson, N., Kauffmann, H. F. & Mančal, T. Enhancement of vibronic and ground-state vibrational coherences in 2D spectra of photosynthetic complexes. *arXiv* 1211.4397 (2012).

[38] Mančal, T. *et al.* Vibrational wave packet induced oscillations in two-dimensional electronic spectra. II. Theory. *J. Chem. Phys.* **132**, 184515 (2010).

[39] Nemeth, A. *et al.* Vibrational wave packet induced oscillations in two-dimensional electronic spectra. I. Experiments. *J. Chem. Phys.* **132**, 184514 (2010).

[40] Hamer, F. M. *The Cyanine Dyes and Related Compounds* (Wiley & Sons, London, U.K., 1964).

[41] Mushkalo, I. L., Dyadyusha, G. G. & Turova, L. S. A macrocyclic bis-cyanine dye. *Tetrahedron Lett.* **21**, 2977–2980 (1980).

[42] Mushkalo, I. L., Sogulyaev, Y. A. & Tolmachev, A. I. Macrocyclic bisindocarbocyanines. *Ukr. Khim. Zh.* **57**, 1177–1181 (1991).

[43] Prokhorenko, V. I., Halpin, A. & Miller, R. J. D. Coherently-controlled two-dimensional photon echo electronic spectroscopy. *Opt. Express* **17**, 9764–9779 (2009).

[44] Kane, D. J. & Trebino, R. Characterization of arbitrary femtosecond pulses using frequency-resolved optical gating. *IEEE J. Quant. Electron.* **29**, 571–579 (1993).

[45] Quimby, R. *Photonics and Lasers: An Introduction*, chap. 17 (John Wiley & Sons, Inc., Hoboken, NJ, USA, 2006).

[46] Jansen, T. L. C. & Knoester, J. Nonadiabatic effects in the two-dimensional infrared spectra of peptides: Application to alanine dipeptide. *J. Phys. Chem. B* **110**, 22910–22916 (2006).

[47] Torii, H. Effects of intermolecular vibrational coupling and liquid dynamics on the polarized Raman and two-dimensional infrared spectral profiles of liquid N,N-dimethylformamide analyzed with a time-domain computational method. *J. Phys. Chem. A* **110**, 4822–4832 (2006).

[48] Tempelaar, R., van der Vegte, C. P., Knoester, J. & Jansen, T. L. C. Surface hopping modeling of two-dimensional spectra. *J. Chem. Phys.* **138**, 164106 (2013).